Journal of Alloys and Compounds, 206 (1994) 217–224
JALCOM 1042

Coherent phase diagram of the AuCu–Pt section in the Au–Cu–Pt ternary system

A.M. El Araby*
Graduate School of Dental Science, Nagasaki University, Nagasaki 852 (Japan)

Y. Tanaka, K-I. Udoh, K. Hisatsune and K. Yasuda
Department of Dental Materials Science, Nagasaki University School of Dentistry, 1-7-1 Sakamoto, Nagasaki 852 (Japan)

(Received November 2, 1993)

Abstract

To determine the coherent phase diagram of the AuCu–Pt pseudobinary system, phase identification and analysis of microstructural configurations were performed, mainly by means of transmission electron microscopy and selected-area electron diffraction examination. Various regions were found in the present experimental coherent phase diagram: (1) α phase region (a single phase of f.c.c. disordered solid solution); (2) AuCu I ($L1_0$), f.c.t. ordered single-phase region; (3) long-period orthorhombic superstructure AuCu II ($L1_{0-S}$) single-phase region; (4) α+AuCu I region of two coexisting phases; (5) AuCu I+AuCu II region of two coexisting phases; (6) α+AuCu I+AuCu II region of three coexisting phases. Microstructural features of these regions were described related to phase transformations.

1. Introduction

At present, it is well known that desirable mechanical properties in dental gold alloys containing platinum and/or palladium are obtained by controlling phase transformations brought about by appropriate heat treatment, *i.e.* age hardening. The characteristics of the age hardening and related phase transformations have been studied using transmission electron microscopy (TEM) and selected-area electron diffraction (SAED) techniques by the present authors [1–7]. It has been shown that the age hardening in commercial dental gold alloys resulted from the formation of AuCu I ordered nuclei on the disordered matrix {100} planes. In adjacent ordered platelets of AuCu I, the *c* axes were mutually perpendicular, to compensate for the strain induced by their tetragonality. Twinning also took place on the $(101)_{tet}$ plane, to relieve the strain caused by the tetragonal distortion in the ordered domain. The nodular precipitates that formed at grain boundaries did not play an important role in the age hardening.

Phase transformations in Au–Cu–Ag ternary alloys have been elucidated to understand the age hardening mechanisms in dental gold alloys by means of TEM, SAED [8–17] and high resolution electron microscopy (HREM) [18–21], because these ternary alloys are thought to be fundamental alloys for commercial dental gold alloys, even though they are composed of five or more constituents. During the course of the systematic investigation to elucidate the phase transformations in Au–Cu–Ag ternary alloys, Nakagawa and Yasuda [22] determined a coherent phase diagram of the $Au_X-(Ag_{0.24}Cu_{0.76})_{1-X}$ section in this ternary system, and confirmed it by comparison with a theoretical coherent phase diagram of the same vertical section in the Au–Cu–Ag ternary system calculated using the cluster variation approximation of Yamauchi [23].

According to the hypothesis of Allen and Cahn [24], a coherent phase must be metastable and, in the presence of the incoherent phase, must be unstable. Coherency strain must also be present in the coherent multiphase structure, and dislocation must be visible at the interfaces with the incoherent phase to reduce coherency strain. They showed that the coherent phase diagram of the Fe–Al binary system could be obtained by TEM, as long as the study satisfied their hypothesis [24]. Therefore, a coherent phase diagram gives us more effective information to predict phase transformations related to age hardening characteristics in an alloy system than does an equilibrium phase diagram.

Thus, the aim of the present study is to determine a coherent phase diagram of the AuCu–Pt pseudobinary system, and to elucidate the role of platinum in phase

*On leave from School of Dentistry, Alexandria University, Alexandria, Egypt.

SSDI 0925-8388(93)01042-3

transformations related to age hardening in dental gold alloys.

2. Experimental procedure

Eight alloys (the compositions and lattice parameters of their solid solution shown in Table 1) were prepared from pure materials of better than 99.95% purity, by melting under a nitrogen atmosphere. The ingots were cold rolled into sheet 0.5 mm thick and then subjected several times to annealing. Discs 3 mm in diameter were punched out from thin foils 0.07 mm thick, subjected to solution treatment at 973 K for 3.6 ks under an argon atmosphere, and then quenched into ice brine to obtain a single phase of disordered solid solution. These discs were then aged in evacuated silica tubes at different temperatures for different periods to produce phase transformations.

They were electrothinned to transparency by a double-jet technique in a solution of 200 g chromium trioxide in 1000 ml of acetic acid and 100 ml distilled water. A 200 kV transmission electron microscope equipped with a specimen-tilting device was employed, with symmetrical illumination along the [010] zone. Analysis of the observed structural features was carried out by the correlation of bright- and dark-field TEM images with SAED patterns.

3. Results and discussion

3.1. Experimental coherent phase diagram

Figure 1 shows a coherent phase diagram of the AuCu–Pt pseudo binary system depicted on the basis of the present TEM and SAED examinations. The cross symbols in Figs. 1 and 2 show the critical temperatures for ordering in each alloy, obtained from an electrical resistivity measurement during continuous heating and cooling at a constant rate of 1.67 mK s^{-1}. It is clear that the critical temperature was elevated slightly with an increase in the platinum content of the alloy within the composition range of approximately 1.3 at.% Pt, *i.e.* the formation region of the AuCu II ordered phase. With a further increment in the platinum content, the critical temperature rose considerably, *e.g.* to 900 K for AuCu–6.92at.%Pt alloy.

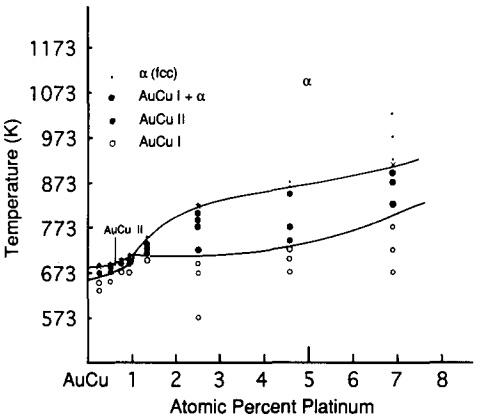

Fig. 1. Experimental coherent phase diagram of the AuCu–Pt pseudobinary system.

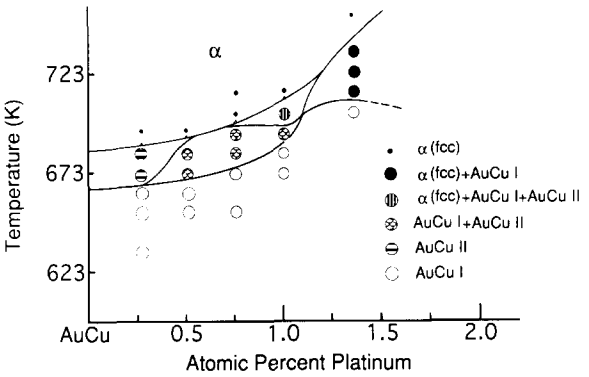

Fig. 2. Enlargement of the coherent phase diagram shown in Fig. 1.

It can be seen that the phase diagram consists of four distinguishable phase regions: a single-phase region of disordered solid solution, *i.e.* α (f.c.c.); a phase region of long-period orthorhombic superstructure AuCu II ($L1_{0-S}$); a single-phase region of AuCu I, f.c.t. ordered ($L1_0$); a region of coexisting disordered α and AuCu I ordered phases. Although the AuCu I formation region extends widely, the AuCu II region is restricted in narrow composition and temperature ranges, and the AuCu II ordered region disappears on the phase diagram in the composition range over approximately 1.3 at.% Pt. Furthermore, the AuCu II region is divided into three different phase regions on the basis of the TEM and SAED examinations, as shown in Fig. 2. Thus, six distinguishable phase regions are found: (1) a disordered solid solution α single-phase region; (2)

TABLE 1. Chemical composition of alloys and their lattice parameter after solution treatment

Alloy	Composition (at.%)			Lattice parameter (nm)
	Au	Cu	Pt	
No.1	50.00	50.00	–	0.38753
No.2	49.85	49.89	0.26	0.38747
No.3	49.76	49.73	0.51	0.38747
No.4	49.64	49.60	0.76	0.38747
No.5	49.47	49.56	0.97	0.38754
No.6	49.84	48.80	1.35	0.38758
No.7	48.85	48.67	2.48	0.38762
No.8	49.97	45.33	4.69	0.38874
No.9	46.50	46.57	6.92	–

a single-phase region of long-period superstructure AuCu II; (3) a single-phase region of superstructure AuCu I; (4) AuCu I + AuCu II region of two coexisting phases; (5) AuCu I + AuCu II + α region of three coexisting phases; (6) α + AuCu I region of two coexisting phases.

3.2. Microstructural features and phase identification

3.2.1. Single-phase region of AuCu I

An SAED pattern taken from a specimen of AuCu–0.97at.%Pt alloy aged at 673 K for 100 ks, and its schematic representation are shown in Figs. 3(a) and 3(b) respectively. The appearance of superlattice reflections, *i.e.* 001_X, 001_Y and equivalent positions, suggests the formation of an $L1_0$-type superlattice of AuCu I f.c.t. in structure. The Miller indices of hkl_X and hkl_Y refer to the X and Y directions, which correspond here to the horizontal and vertical directions in the figure respectively. The full semicircles show the direction of the c axis in the f.c.t. diffraction pattern of AuCu I. Furthermore, an SAED pattern is obtained by the superposition of two different orientation variants of the AuCu I diffraction pattern, by a simple rotation of 2ϕ about the central circle, *i.e.* direct spot in the SAED pattern, as seen in Fig. 3(b). Here, the rotation angle ϕ is given by

$$\tan(\pi/4 - \phi) = c/a$$

according to Yamaguchi [25]. This configuration of spots in the SAED pattern indicates twinning, which is the result of tetragonal distortion.

Dark-field images produced using the 001_X and 001_Y superlattice reflections are shown in Figs. 3(c) and 3(d) respectively. The microstructure exhibits two well-oriented sets of alternating dark and bright coarse bands, which are parallel to the [101] direction, *i.e.* twin boundary, in Figs. 3(c) and 3(d). From the configuration of the diffraction spots in the SAED pattern, these coarse bands are identified as twin platelets of AuCu I, induced by tetragonal distortion.

The bright coarse bands contain fine dark stripes which are thought to be antiphase domain boundaries (APBs) induced thermally during ordering. By comparing the direction of the APB planes in Fig. 3(c) with those in Fig. 3(d), it is clear that these APB planes should be conservative, because they are located parallel to the c axis of AuCu I ordered phase.

Fig. 4 shows TEM images and an SAED pattern taken from a specimen of AuCu–6.92at.%Pt alloy aged at 673 K for 100 ks. The microstructure represents two sets of orientation variants of twin platelets which intersect one another, as can be seen in the central portion of Fig. 4(a). This configuration is confirmed clearly by inspection of the dark-field images shown in Figs. 4(b) and 4(c), which are produced using the 001_X and 001_Y superlattice reflections respectively. However, narrow and short bands observed in the central portion of the micrographs disappeared as a result of lengthy aging at 673 K for 3 Ms. Then, only alternating dark and bright coarse bands remained in the whole area of the crystal. In Figs. 4(b) and 4(c), fine dark stripes are also found in the bright bands, as seen in Figs.

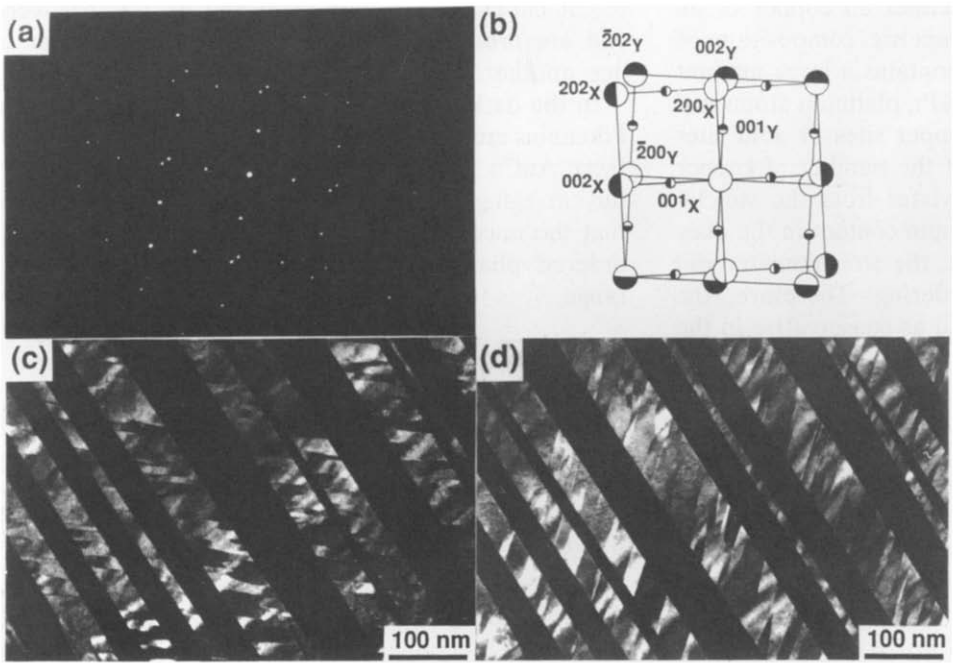

Fig. 3. TEM images and SAED pattern of AuCu–0.97at.%Pt alloy aged at 673 K for 100 ks: (a) [100] SAED pattern; (b) schematic representation of the SAED pattern; (c), (d) dark-field images produced using 001_X and 001_Y superlattice reflections respectively.

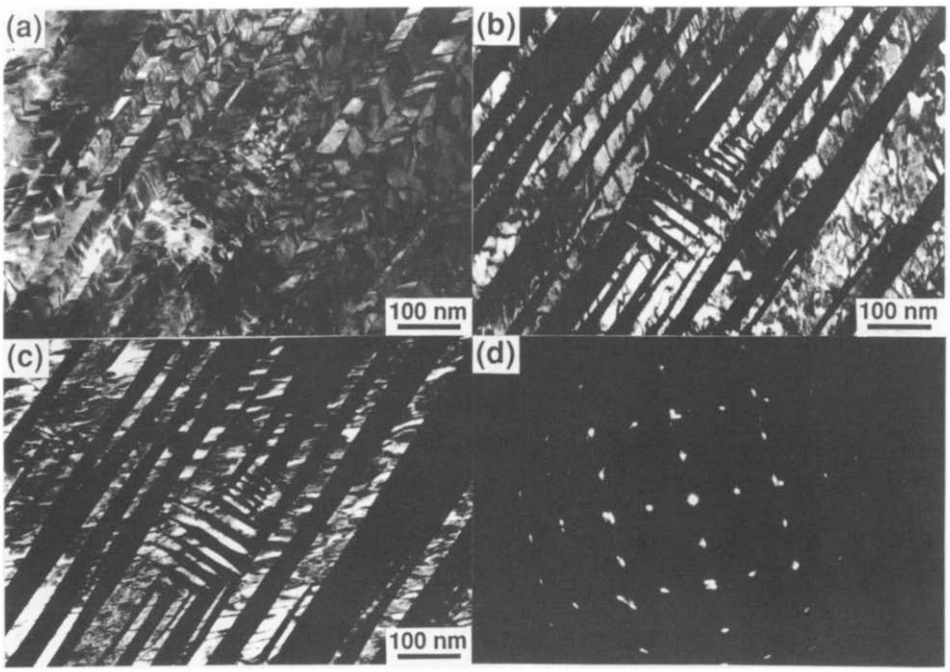

Fig. 4. TEM images and SAED pattern of AuCu–6.92at.%Pt alloy aged at 673 K for 100 ks: (a) bright-field image; (b), (c) dark-field images produced using 001_X and 001_Y superlattice reflections respectively; (d) [001] SAED pattern.

3(c) and 3(d). It is apparent in Figs. 4(b) and 4(c) that the thermal APB planes lie perpendicular to the *c* axis of the AuCu I ordered phase. Thus, it is thought that these APBs are non-conservative APBs.

The conservative APB was formed during ordering in AuCu–0.97at.%Pt alloy, while the non-conservative APB was found in AuCu–6.92at.%Pt alloy. The stable structure for the AuCu I alloy is f.c.t. and alternate (002) planes are occupied by either all copper or all gold atoms to give a stoichiometric composition of Au–Cu alloy. When the alloy contains a large amount of platinum, *e.g.* AuCu–6.92at.%Pt, platinum atoms will occupy preferentially either copper sites or gold sites in the superlattice; the ratio of the number of copper planes to gold planes then deviates from the stoichiometry. In contrast, if the platinum content in the alloy is small, *e.g.* AuCu–0.97at.%Pt, the stoichiometry will be maintained during the ordering. Therefore, the thermal APB can be maintained as conservative in the ordered phase.

3.2.2. Single-phase region of AuCu II

Figures 5(a) and 5(b) respectively show an SAED pattern taken from a specimen of AuCu–0.26at.%Pt alloy aged at 673 K for 100 ks and its schematic representation. The superlattice reflections, *i.e.* the 001 and equivalent positions, split into two spots, resulting in $0\ \frac{1}{2}M\ 1$ and $0\ -\frac{1}{2}M\ 1$ superlattice reflections. This configuration in the SAED pattern is characteristic of the formation of the long period antiphase boundary (LPAPB) AuCu II ordered phase observed in the SAED pattern. Here, the notation *M* indicates the periodic antiphase domain size.

Two dark-field TEM images produced using the 001_X and 001_Y superlattice reflections are shown in Figs. 5(c) and 5(d) respectively (for convenience, Miller indices are used in terms of AuCu I). These indicate the presence of LPAPBs with twinning. The ordered domains of the *X* and *Y* variants correspond to the bright bands seen in Figs. 5(c) and 5(d) respectively, and are arranged with their *c* axes perpendicular to one another.

In the dark-filled images, some small areas of AuCu I domains are visible as plain contrast regions. However, these AuCu I domains are transformed to AuCu II by further aging for 3 Ms at 673 K. Thus, it is identified that the microstructure consisted of only the AuCu II ordered phase in this composition and temperature range.

3.2.3. Region of two coexisting phases AuCu I and AuCu II

An SAED pattern taken from a specimen of AuCu–0.51at.%Pt alloy aged at 673 K for 100 ks and its schematic representation are shown in Figs. 6(a) and 6(b) respectively. The simultaneous appearance of the 001, $0\ \frac{1}{2}M\ 1$, $0\ -\frac{1}{2}M\ 1$ and equivalent superlattice reflections indicates the coexistence of the AuCu I and AuCu II ordered phases. In addition to the above, the superimposed configuration of the SAED pattern suggests the occurrence of twinning. A microstructure which consists of two sets of twin platelets of bright and dark

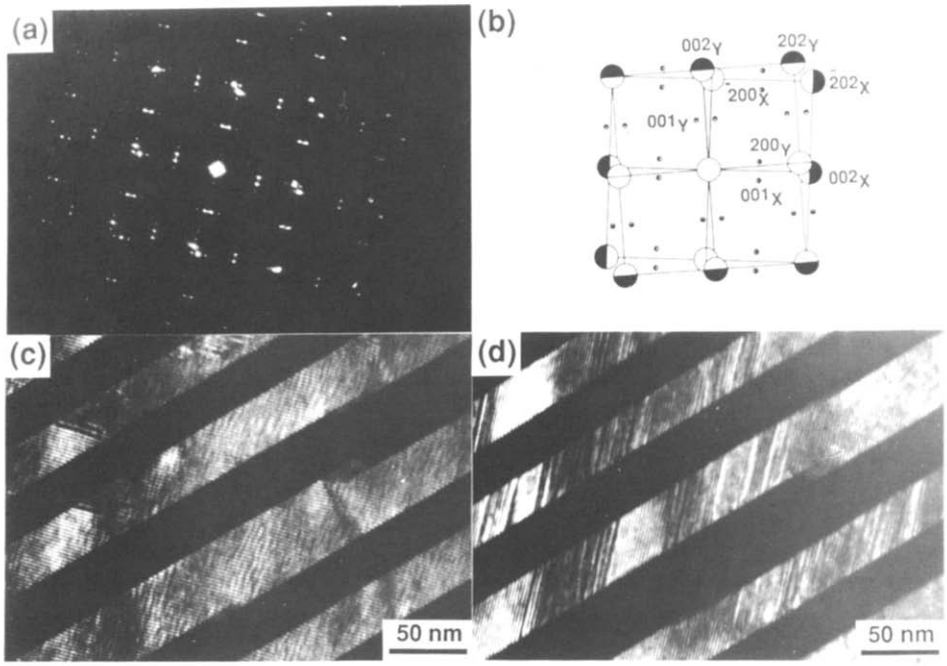

Fig. 5. TEM images and SAED pattern of AuCu–0.26at.%Pt alloy aged at 673 K for 100 ks: (a) [100] SAED pattern; (b) schematic representation of the SAED pattern; (c), (d) dark-field images produced using 001_X and 001_Y superlattice reflections respectively.

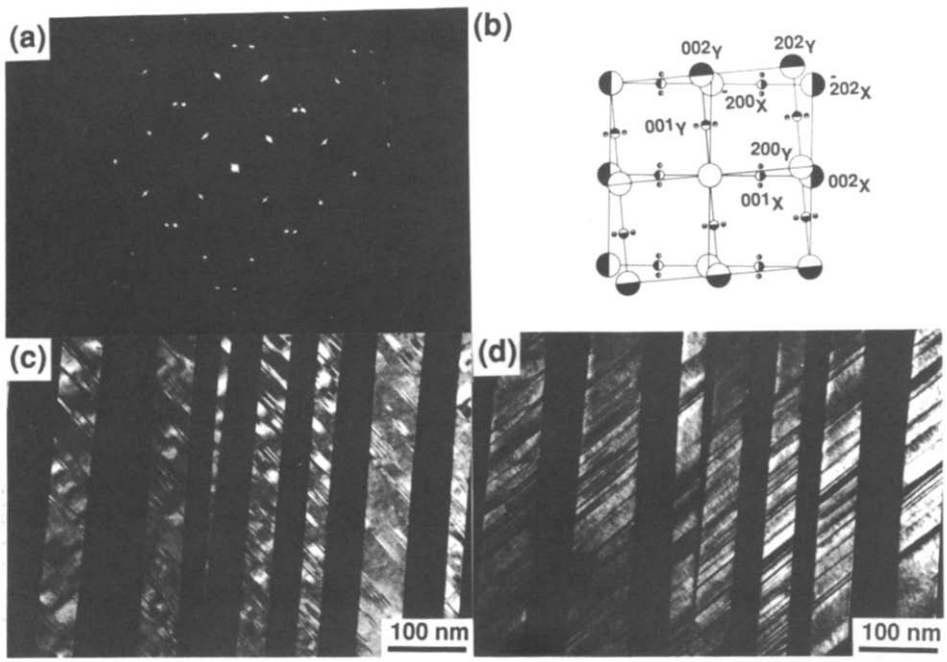

Fig. 6. TEM images and SAED pattern of AuCu–0.51at.%Pt alloy aged at 673 K for 100 ks: (a) [100] SAED pattern; (b) schematic representation of the SAED pattern; (c), (d) dark-field images produced using 001_X and 001_Y superlattice reflections respectively.

bands is the same essentially as those found in Figs. 3–5. However, LPAPBs are visible as parallel black fringes inside the bright bands. In the dark-field images shown in Figs. 6(c) and 6(d), two different regions are distinguished by their contrast, *i.e.* a well-developed LPAPB structure attributed to the AuCu II ordered phase, and areas of plain bright contrast arising from the AuCu I ordered phase. Therefore, it is identified that the coexisting AuCu I and AuCu II ordered phases were formed in this temperature range.

3.2.4. Region of two coexisting phases α and AuCu I

Figure 7 shows TEM images and an SAED pattern taken from a specimen of AuCu–6.92at.%Pt alloy aged

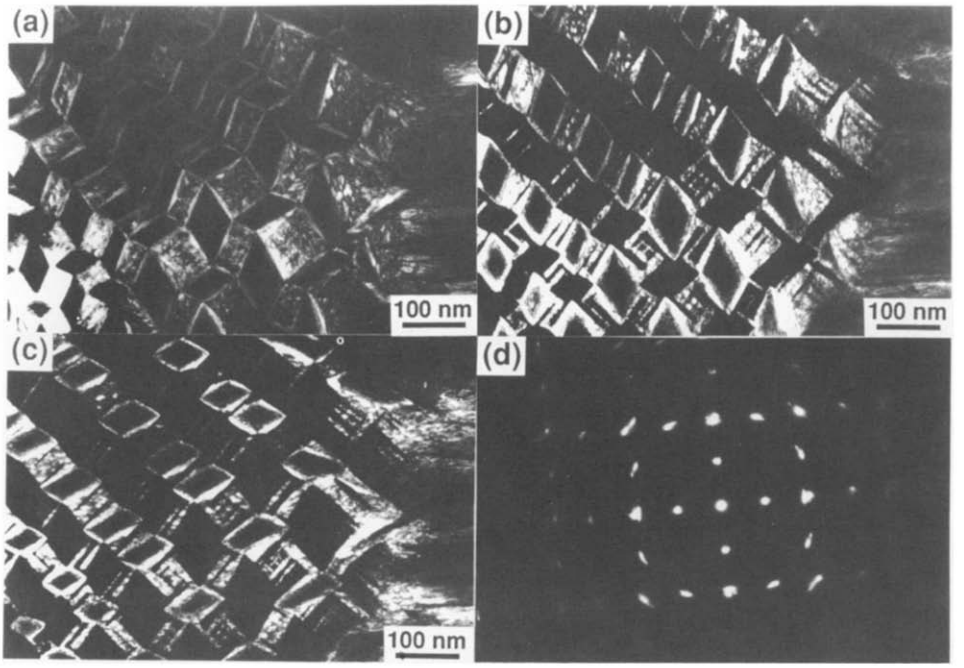

Fig. 7. TEM images and SAED pattern of AuCu–6.92at.%Pt alloy aged at 893 K for 100 ks: (a) bright-field image; (b), (c) dark-field images produced using 001_X and 001_Y superlattice reflections respectively; (d) [001] SAED pattern.

at 893 K for 100 ks. In a bright-field image (Fig. 7(a)), it can be observed that a characteristic microstructure similar to the checkered pattern consists of a number of scattered cuboidal blocks and surrounding parallelogram-shaped regions. The dark-field images shown in Figs. 7(b) and 7(c), which were produced using the 001_X and 001_Y superlattice reflections respectively, indicate that these parallelogram-shaped regions are composed of two different orientation variants of the AuCu I ordered phase. This is even though the ordered phase is brightened only in the peripheral region, since the cuboidal blocks are thinned more preferentially than the parallelogram-shaped regions by electrothinning. It is thought that the cuboidal blocks can be identified as disordered α phase, as will be shown later. It also can be observed that the parallel sides of a cuboidal block are in contact with an orientation variant of an AuCu I parallelogram – *e.g.* the (001) planes of the *X* variant of an AuCu I parallelogram contact with the (100) planes of the cuboidal block – and the other sides of the cuboidal block are adjacent to a different orientation variant of the AuCu I parallelogram – *e.g.* the (001) planes of the *Y* variant of an AuCu I parallelogram contact with the (010) planes of the cuboidal block [21].

In the dark-field images, it is apparent that the cuboidal blocks contain fine mottled contrast. It is thought that this contrast was generated by fine ordered particles induced during quenching from the aging temperature (in the present case, at 893 K) to ice brine [26]. Therefore, the cuboidal blocks are essentially disordered α phase but contain fine ordered particles which have a twin relationship with one another. This situation will be explained by an analysis of the SAED pattern.

Figure 8(a) shows a schematic representation of the SAED pattern originated from the parallelogram-shaped AuCu I ordered regions, which consists of the *X* and *Y* variants of AuCu I. In contrast, the SAED pattern of the cuboidal blocks shown in Fig. 8(b) was obtained by the superposition of Fig. 8(a) with a simple rotation of 2ϕ about the direct spot, as observed in Figs. 3(a) and 3(b). This analysis was carried out on the basis of HREM observations; however, the HREM results will be published elsewhere in the near future. Figure 8(c) is a superposition of Figs. 8(a) and 8(b), and is in good agreement with Fig. 7(d). Thus, it is demonstrated that coexisting α disordered and AuCu I ordered phases were formed in this temperature range.

3.2.5. Region of three coexisting phases α, AuCu I and AuCu II

Figure 9 shows TEM images and an SAED pattern taken from a specimen of AuCu–0.97at.%Pt alloy aged at 703 K for 1 Ms. A bright-field image (Fig. 9(a)) shows a microstructure consisting of bands intersected with one another and their matrix. These bands are bright only in the dark-field image produced using the 001_X superlattice reflection, as seen in Fig. 9(b). However, the matrix appears as bright regions only in the dark-field image produced using the 001_Y superlattice

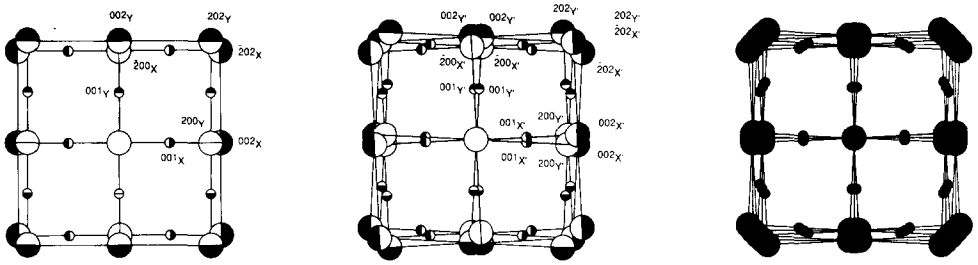

(a) (b) (c)

Fig. 8. Schematic representation of the SAED pattern shown in Fig. 7(d): (a) schematic representation of the SAED pattern from ordered regions formed by aging at 893 K for 100 ks in the parallelogram-shaped region; (b) schematic representation of the SAED pattern from the ordered particles formed during quenching from 893 K to ice brine in the cuboidal blocks; (c) superimposed SAED pattern of (a) and (b).

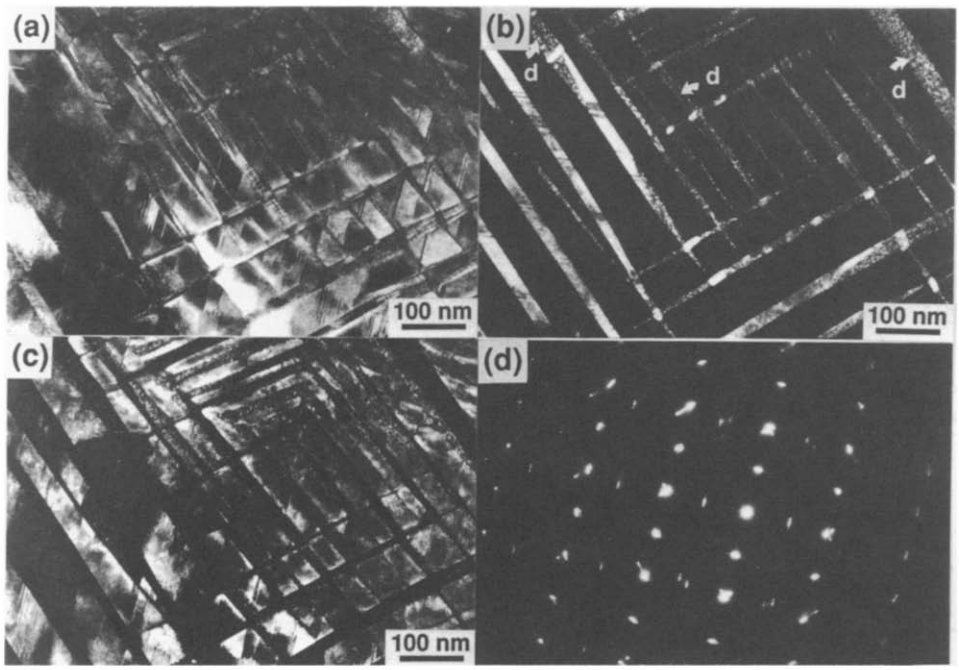

Fig. 9. TEM images and SAED pattern of AuCu–0.97at.%Pt alloy aged at 703 K for 1 Ms: (a) bright-field image; (b), (c) dark-field images produced using 001_X and 001_Y superlattice reflections respectively; (d) [001] SAED pattern.

reflection, as seen in Fig. 9(c). Both the bands and the matrix fill their gaps mutually. In addition, they contain not only the LPAPB structure of AuCu II but AuCu I also exists, as can be seen in regions showing plain contrast. The SAED pattern shown in Fig. 9(d) also supports this observation, because the 001 and equivalent superlattice reflections can be recognized, in addition to the split reflections characteristic of the LPAPB structure of AuCu II.

In Fig. 9(b), regions showing a fine mottled contrast are observed as indicated by the arrow and letters d. It is thought that this fine mottled contrast can be attributed to the ordered particles induced unavoidably by quenching from the aging temperature to ice brine, as seen in Figs. 7(b) and 7(c). However, the ordered particles are thought to be essentially a disordered phase. Thus, a region with three coexisting phases, *i.e.* the α disordered, AuCu I and AuCu II ordered phases, is identified within a narrow temperature and composition range, as seen in Fig. 2.

Figure 10 represents part of a plausible isothermal section at 673 K of the Au–Cu–Pt coherent phase diagram [27]. By using this plausible phase diagram, it can be explained that the sequence of the appearance of the phase regions varies according to the platinum content in the alloys. On the isothermal line at 673 K drawn in Fig. 2, we can observe a single-phase region of AuCu II in AuCu–0.26at.%Pt alloy. With increasing platinum content in the alloy, a region of two coexisting phases AuCu I and AuCu II was formed. Then, a single-phase region of AuCu I appeared with a further increment in the platinum content in the alloy. In-

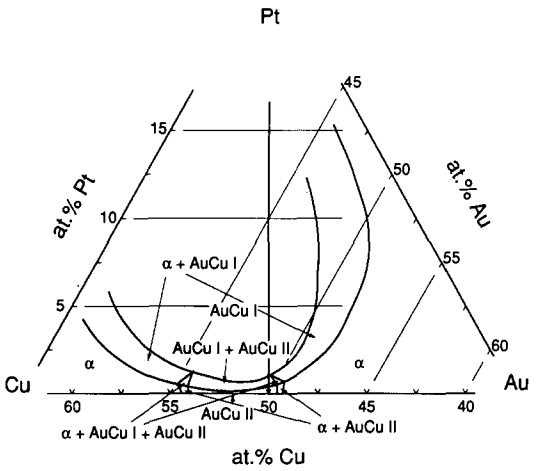

Fig. 10. Isothermal section of a plausible phase diagram of Au–Cu–Pt system.

spections of Fig. 2 agree with those in Fig. 10. Thus, we can reasonably propose the present coherent phase diagram of the AuCu–Pt pseudobinary system.

Acknowledgment

The authors gratefully acknowledge the financial support of the present work through a Grant-in-Aid for scientific research (Grant 03452277) from the Japanese Ministry of Education, Science and Culture.

References

1 A. Prasad, T. Eng and K. Mukherjee, *Mater. Sci. Eng., 24* (1976) 179.
2 K. Yasuda and M. Ohta, *J. Less-Common Met., 70* (1990) 75.
3 K. Yasuda, K. Udoh, K. Hisatsune and M. Ohta, *Dent. Mater. J., 2* (1983) 48.
4 K. Udoh, K. Hisatsune, K. Yasuda and M. Ohta, *Dent. Mater. J., 3* (1984) 253.
5 K. Udoh, K. Yasuda and M. Ohta, *J. Less-Common Met., 118* (1986) 249.
6 K. Yasuda, G. Van Tendeloo, J. Van Landuyt and S. Amelinckx, *J. Dent. Res., 65* (1986) 1179.
7 T. Tani, K. Udoh, K. Yasuda, G. Van Tendeloo and J. Van Landuyt, *J. Dent. Res., 70* (1991) 1350.
8 Y. Kanzawa, K. Yasuda and H. Metahi, *J. Less-Common Met., 43* (1975) 121.
9 K. Yasuda, H. Metahi and Y. Kanzawa, *J. Less-Common Met., 60* (1978) 65.
10 K. Yasuda and Y. Kanzawa, *Trans. Jpn. Inst. Met., 18* (1977) 46.
11 K. Yasuda and M. Ohta, Age-hardening in a 14 carat dental gold alloy, *Proc. 3rd Int. Precious Metals Conf., Chicago, IL,* International Precious Metals Institute, 1979, pp. 137–164.
12 K. Yasuda and M. Ohta, *J. Dent. Res., 61* (1982) 473.
13 M. Ohta, T. Shiraishi, M. Yamane and K. Yasuda, *Dent. Mater. J., 2* (1983) 10.
14 M. Nakagawa and K. Yasuda, *Phys. Status Solidi A, 107* (1988) 709.
15 M. Nakagawa and K. Yasuda, *J. Mater. Sci., 23* (1988) 2975.
16 K. Hisatsune, K. Udoh, B.-I. Sosrosoedirjo, T. Tani and K. Yasuda, *J. Alloys Comp., 176* (1991) 301.
17 K.-I. Udoh, H. Fujiyama, K. Hisatsune, M. Hasaka and K. Yasuda, *J. Mater. Sci., 27* (1992) 504.
18 K. Yasuda, M. Nakagawa, G. Van Tendeloo and S. Amelinckx, *J. Less-Common Met., 135* (1987) 169.
19 K. Yasuda, M. Nakagawa, K. Udoh, G. Van Tendeloo and J. Van Landuyt, *J. Less-Common Met., 158* (1990) 301.
20 K. Udoh, K. Yasuda, G. Van Tendeloo and J. Van Landuyt, *J. Alloys Comp., 176* (1991) 147.
21 K. Yasuda, K. Hisatsune, K.-I. Udoh, Y. Tanaka, G. Van Tendeloo and J. Van Landuyt, *Dent. Jpn., 29* (1992) 91.
22 M. Nakagawa and K. Yasuda, *J. Less-Common Met., 138* (1988) 95.
23 H. Yamauchi, Private communication, 1984.
24 S.M. Allen and J.W. Cahn, *Acta Metall., 23* (1975) 1017.
25 S. Yamaguchi, *Jpn. J. Appl. Phys., 5* (1966) 496.
26 Y. Tanaka, K.-I. Udoh, K. Hisatsune and K. Yasuda, *Philos. Mag.,* in press.
27 E.I. Maluff and R.W. Cahn, *J. Less-Common Met., 114* (1985) 65.